Proceedings of ASME Turbo Expo 2023: Turbomachinery Technical Conference and Exposition
GT2023
June 26-30, 2023, Boston, MA

GT2023-100642

STRATEGIES FOR HIGH-ACCURACY MEASUREMENTS OF STAGE EFFICIENCY FOR A COOLED TURBINE

Maria Rozman, Reid A. Berdanier,
Michael D. Barringer, and Karen A. Thole

Pennsylvania State University
Steady Thermal Aero Research Turbine Lab
University Park, PA 16802, USA

ABSTRACT

Gas turbines are used in a broad range of aerospace and land-based applications from power generation to aviation, and their usage is projected to continue to grow. As a result, it is critical to find innovative solutions for improving turbine efficiency to reduce fuel consumption and carbon emissions. Successful demonstration of new efficiency-increasing technologies at rig or engine scale requires efficiency measurement techniques that are both accurate and repeatable. The Steady Thermal Aero Research Turbine (START) Laboratory at the Pennsylvania State University is utilizing a unique 360° traversing system for temperature and pressure probes with redundant torque measurements to quantify thermal efficiency for a single-stage cooled test turbine. The purpose of this study is to determine a measurement method that produces highly accurate and repeatable efficiency calculations. With these systems, flows in the full annulus have been analyzed and compared with subsector traverse segments centered at different circumferential positions to determine the appropriate sector size. The results from this investigation indicate that the full 360° measurement is recommended to minimize variation in calculated stage efficiencies. This study also compares the circumferential variations in thermodynamic and mechanical efficiency calculation methods, finding that the thermodynamic efficiency calculation results in a higher accuracy for full exit plane measurements. In parallel, a statistical analysis was performed to determine the number of required repeats for the full 360° traverse necessary to achieve a desired precision uncertainty that is half of the bias uncertainty. Ultimately, this study establishes guidelines to streamline experimental procedures by limiting the necessary test count per operating condition to 10 measurements. Following these procedures establishes a bias of ε_b = 0.18 points, and limits the precision uncertainty to at most ε_p = 0.09 points, resulting in a total uncertainty of at most ε_t = 0.20 points.

NOMENCLATURE

B	Rig Build
C_p	Discharge Coefficient
h	Enthalpy
$\dot{m}$	Mass flow rate
n	Sample size/count
N	Wheel speed
p	Pressure
P	Plane
t	Student's t-distribution
T	Temperature
X	Varied Operating Parameter

Greek

ε	Uncertainty
η	Efficiency
Δ	Difference
θ	Sector size
ϕ	Circumferential location
σ	Standard deviation
τ	Torque

Subscripts, Abbreviations, and Accents

1,2	Stage locations, enumerations
b	Bias
c	Cooling flow
BDC	Bottom dead center
BL	Baseline
CFD	Computational fluid dynamics
CI	Confidence interval
dyno	Dynamometer
MGP	Main gas path
p	Precision
purge	Purge
PDF	Probability density function
PR	Pressure ratio

RPM	Revolutions per minute
RSS	Root sum square
RTD	Resistance temperature detector
s	Isentropic value
START	Steady Thermal Aero Research Turbine
t	Total value
TC	Thermocouple
TDC	Top dead center
TOBI	Tangential onboard injection
tqm	Torquemeter
VTE	Vane trailing edge

INTRODUCTION

An examination of the Brayton cycle shows that increasing turbine inlet temperature increases the cycle efficiency of a gas turbine engine. As developments in the combustor meet these temperature demands, technology downstream in the engine, namely the turbine, must develop strategies to protect the components from deterioration to maintain blade life [1]. Cooling flows redirected from the compressor are commonly used for this purpose, however redirecting compressor bleed air as coolant for turbine hardware is known to cause deleterious impacts on turbine performance [2–5].

In order to properly design engines, it is important to quantify the exact impact of cooling flows on both the durability and efficiency of turbines. The best way to develop these strategies is using scaled turbine test rigs to isolate changes in cooling design. It is of the utmost importance for sustainable aviation to optimize for turbine efficiency, as even small improvements to efficiency can have huge impacts on fuel consumption, and NO_x and CO_2 emissions [6,7]. Therefore, it is critical to ensure that the methods used to experimentally quantify performance are both the best physical representation of the system as well as accurate, repeatable, and reliable.

An analysis of uncertainty is critical to building accuracy in experimental results, as well as lending insight into tracing potential sources of error in instrumentation data precision to help guide the development of more robust testing methods. This paper uses the framework of an in-depth uncertainty analysis to optimize data acquisition methods and testing protocols for the measurement of stage efficiency in a single stage cooled turbine test rig.

LITERATURE REVIEW

Turbine performance is often quantified as a record of losses that are attributed to viscous effects from boundary layers or mixing, shock waves, heat transfer, endwall losses, tip leakage losses, drag, cooling and mixing from sealant flows, windage losses, and other fluid dynamics [4]. These types of losses are proportional to entropy generation. While entropy is not measured directly, change in entropy, or entropy generation, can be examined using thermodynamic properties. Young and Wilcock [8] quantified loss using entropy generation and examined the impacts of different cooling flows in detail on turbine performance. These methods were applied computationally by Yoon et al. [9] through a loss audit using this proportional entropy generation method on steady and unsteady Computational Fluid Dynamics (CFD) cases. Experimentally, cascade test data or empirical correlations were commonly used to estimate the loss coefficient using stagnation pressure loss [4], but without rotating test rigs, not all effects of relative motion of the blades and associated endwall losses can be fully captured.

Alternatively, turbine performance can be determined in the form of adiabatic efficiency, defined as the ratio of actual work generated by the turbine to the ideal work produced by an isentropic expansion. This method typically requires measurements of temperatures, pressures, and mass flow rates at the inlet and outlet of the stage to calculate changes in enthalpy [5,8,10–17]. Many studies have extended this thermodynamic, enthalpy-based method to include multiple inlets in cooled turbines [12–14,18]. Louis et al. [12] introduced an enthalpy-based method to calculate efficiency for cooled turbines and later studies such as Horlock and Torbidoni [14], Young and Horlock [19], and Kurzke [18] discuss the multiple configurations and assumptions that could be involved in aerodynamic definitions of efficiency. Berdanier [13] expands on this by foregoing a well-mixed assumption and examining the stage efficiency of a cooled turbine test rig in detail by using different methodologies to average the nonuniform flow at the exit of the turbine. This study will build upon previous cooled turbine efficiency work by interrogating the sensitivity of efficiency to the proportion of the exit plane used as an input to the enthalpy-based efficiency calculation.

There is an alternative method of calculating the actual work in an enthalpy-based efficiency equation. This mechanical method of calculating actual work requires the additional measurement of speed and torque, though the ideal work calculation is identical to that of the thermodynamic method and therefore high-quality measurements of thermodynamic properties are still required. Beard et al. [15] uses this mechanical definition of actual work, but addresses that the torque measurement must be a sum of multiple corrections, including those from windage, drag, and friction from the bearings. This study is an example of one which was conducted at a short duration facility, requiring a variety of temperature, heat flux, and mass flow rate corrections. In his exploration of definitions of efficiency, Kurzke [18] warns of the dubiousness of such definitions, due to the ambiguous inclusions of disk windage and bearing losses in the shaft power term. Several other studies [2,3,5] use the mechanical definition of actual work in their definition of efficiency and use this approach to investigate the impacts of cooling flows on turbine performance alongside numerical and computational methods to track entropy generation and other losses. This study uses the mechanical method to examine the losses generated by different flow physics in a single stage turbine test rig.

Some studies have applied both methods and used the opportunity to compare definitions using a number of metrics including uncertainty and capturing of losses. Hudson and Coleman [11] and by Neumeyer et al. [16] compare the thermodynamic and mechanical methods but stop short of providing a detailed comparison of uncertainty resulting from

the two strategies. Porreca et al. [17] applied the mechanical method in order to examine the efficiency of a two-stage test turbine but also applied a thermodynamic efficiency definition to examine radial variations specifically. This study also compares the relative uncertainties of these two methods, finding the difference to be on the order of 1%. The present study compares the efficiency calculation methods of both the thermodynamic and mechanical definitions of work using a thorough uncertainty analysis while also using statistical methods to drive future testing guidelines.

Depending on the scope of the experimental facility, it is not always feasible or possible to measure the entire circumference of the inlets and outlet of the turbine. Many facilities use only limited or even singular radial measurements as representatives of the turbine profiles [20–22]. Some studies attempt to reconstruct exit conditions from limited radial measurements in order to circumvent this limitation, as Lou did for the exit of a combustor [22]. Seshadri et al. [20,21] conducted a study examining whether temperature flow fields can be accurately described with discrete radial measurements, using Bayesian mass averaging techniques. Facilities such as the Steady Thermal Aero Research Turbine (START) lab are able to use sophisticated traverse systems [23]. The present study leverages a fully-characterized 360° exit plane to examine the impact of sector size and circumferential location on the resulting efficiency calculation, effectively measuring the impact of circumferential nonuniformities that are insufficiently captured by typical limited instrumentation approaches.

Value in experimental data is not derived from sophisticated instrumentation and expensive facilities in isolation. There are multiple motivating purposes for uncertainty analysis including improving instrumentation and procedures, providing a basis for the guarantee of accuracy, and giving validity to the test-parameter range [24]. Uncertainty quantification is almost as essential to presenting results as the data itself, often given as a range about the measured sample mean in which the true hypothetical performance must lie. Analyses typically decompose overall uncertainty into two components: precision and bias, combined together in a root sum square (RSS). Bias is defined as the inherent offset of a physical measurement from the hypothetical true value due to the instrumentation [24–28]. The bias uncertainty of a calculated value such as efficiency requires the quantification of bias for each measured value and the propagation through the given function. This method was developed originally by Kline and McClintock [28] for single sample experiments; these guidelines were further expanded by other researchers such as Moffat [26], Kline [24], and Phillips et al. [27] for application to multiple-sample experiments or functions without analytical expressions. Many studies have conducted an uncertainty analysis, including in experimental, numerical, and computational research, which demonstrated these benefits for their measurements of thermodynamic properties [20,29]. While bias is unavoidable in experimental data, this study reduces it through calibration and applies it as a threshold value for the precision uncertainty analysis.

In summary, the uncertainty in efficiencies vary dependent upon the methods discussed [15,17,30–34]. A selection of reported uncertainty ranges for efficiency from literature are given by Table 1. All of these studies used uncertainty analysis to benefit their testing procedures, either by identifying previously unknown issues or by adding validity in the results using a confidence interval. Similarly, this study is an investment in the larger body of work at the START facility, intended to close the gap between high accuracy equipment, repeatable measurements, and meaningful data. The majority of previous studies choose one calculation and testing method to characterize their systems, but this study interrogates the established efficiency calculation techniques historically implemented by the START lab to drive high accuracy assessments and reduce error.

EXPERIMENTAL METHODS

This study was conducted at the Steady Thermal Aero Research Turbine (START) Lab. The development of this facility is described in detail in Barringer et al. [23]. This lab is an open-loop facility capable of continuous-duration operation, allowing the system to operate at steady state. The flow is driven by two industrial 1.1 MW (1500 hp) compressors, which supply a maximum of 11.4 kg/s (25 lbm/s) of flow to the system. The flow exits the compressors at a pressure of approximately 480 kPa (70 psia) and 380 K (230°F) before being separated into the main gas path (MGP) and cooling flow streams. The MGP flow is heated using a natural gas burner to up to 675 K (750°F) while the cooling flow streams are cooled using a shell-and-tube heat exchanger down to 273 K (32°F).

This system uses three cooling streams fed to different regions throughout the test section: purge flow, which is sent into the wheel space to cool and seal the rim seal cavity; tangential on-board injection (TOBI) flow, which provides cooling air to the blades; and vane trailing edge (VTE) flow, which supplies the cooling for the vane. In total, these flows use approximately 10% of the flow exiting the compressors.

The rotor is capable of being controlled up to 11,000 revolutions per minute (RPM) using a water brake dynamometer with an accuracy of ±10 RPM about the setpoint. The entire rotor assembly is supported using a magnetic levitation bearing system. The test section consists of a single turbine stage, consisting of real engine hardware. Typical hardware interfaces are defined by interference-fits and pinned interfaces with true position tolerances of 0.05 mm (0.002 inch), preventing misalignment and eccentricity of flow path components. A rendering of this facility is shown in Figure 1.

Table 1. Reported Efficiency Uncertainties (ε)

Year	Citation	Bias	Precision	Total
1991	[31]	0.61-0.8	0.25	0.66-0.84
2000	[32]	0.65	0.25	0.70
2004	[34]	-	0.3	-
2006	[30]	1.2	0.68	1.38
2010	[15]	1.76	0.28	1.78

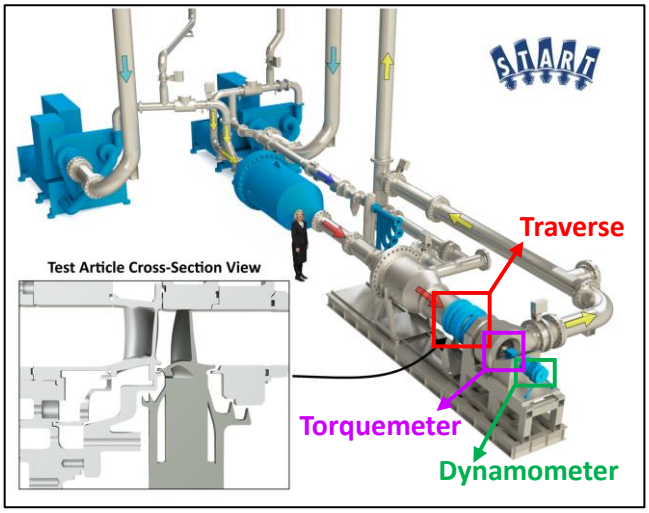

Figure 1. Facility rendering and test article cross-section view, highlighting the instrumentation used to quantify performance.

Facility Instrumentation

There are three instrumentation systems used to calculate efficiency highlighted in Figure 1. The red square is highlighting the test section, which contains the 360° traverse instrumentation system, shown in an illustration in Figure 2.

In this figure, the single stage test section consists of the vane and blade, in light and dark gray respectively. The MGP and each of the cooling flow streams are measured using dedicated Venturi flow meters. The inlet total temperature and pressure measurements are acquired at the midspan in the P_1 inlet plane, located approximately seven axial chords upstream of the vane leading edge, as labelled in Figure 2 using six circumferentially-distributed probes. These fixed measurements are further supplemented by radial traverses at discrete measurement locations approximately 1.5 axial chords upstream of the vane leading edge. The inlet properties of each of the cooling streams were measured at their introduction point to the test section. The total temperatures and pressures at the exit plane were captured using rakes mounted to the 360° traverse, depicted in the illustration in Figure 2 in purple. It should be noted that this figure is not to scale.

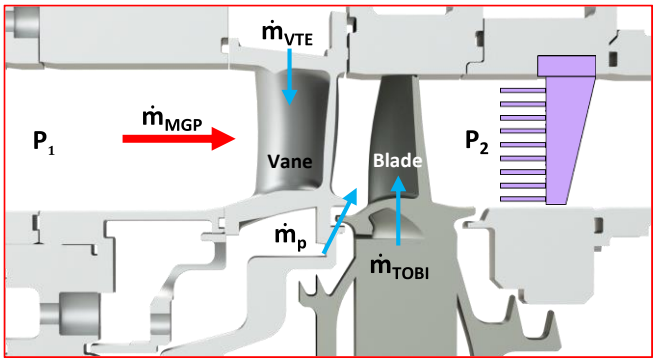

Figure 2. Test article cross section illustration (not to scale), identifying the inputs to the efficiency equation and the traverse rake location with respect to the turbine stage.

The traverse lies on the exit plane P_2, which sits approximately two axial chord lengths downstream of the blade trailing edge. The rake in Figure 2 is one of four equally spaced rakes: two sets of total temperature Kiel probes containing Type-E thermocouples, and two sets of total pressure Kiel probes. Each set consists of one rake with nine sensors spanning from 10% to 90% of the flow path and one rake with 10 sensors spanning 5% to 95% of the flow path.

During operation, this mechanism is capable of traversing the rakes fully about the annulus over the course of about five minutes (equivalent to 0.2 RPM), creating a spatially-resolved map of exit total temperatures and pressures, shown in Figure 3. For the data presented in this study, each test represents more than 300 measurements per full annulus rotation or an average of over 0.8 measurements per degree. Each measurement consists of a time average from a measurement of about one second with a sampling rate of 32 and 90 Hz for the temperature and pressure measurements respectively. The radial measurements are then area- or mass-averaged according to the area averaged equations defined by Berdanier [13] to obtain the input used in the efficiency calculation. These rakes are specifically designed to minimize their impact on the flow field as they traverse. Both sets of rakes were independently calibrated over a range of yaw angles and Mach numbers to determine appropriate recovery factors, which were then subsequently applied to the measured rake data. Because the temperature and pressure probes are located on different instruments, a single circumferential location was measured for each property at different points in time. Due to the steady capabilities of the START lab, the system is able to be held at a set of operating conditions until it becomes "thermally soaked," or reaches thermal steady state. It is therefore

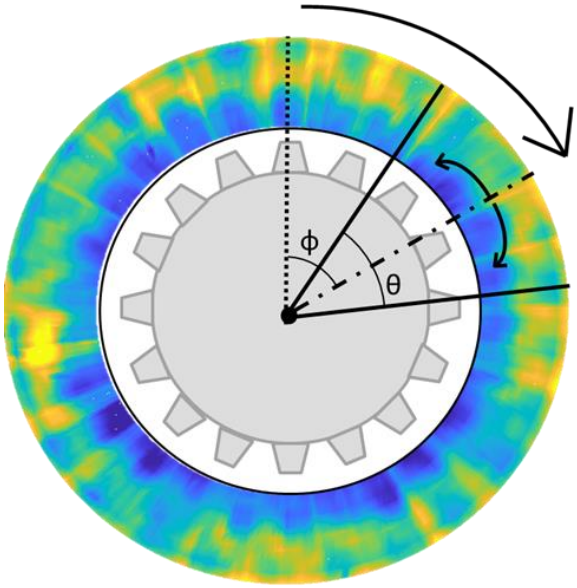

Figure 3. Illustration outlining subsections of the exit plane as a function of sector size, θ, and circumferential location, Φ.

assumed the thermodynamic properties at every point, including the exit plane, are constant with respect to time and time dependent variations are neglected.

This study uses complete 360° exit plane datasets in its examination of limited sector sizes by extracting specified zones from the measured spatial maps of temperature and pressure according to Figure 3. This figure shows an example of the spatially-resolved map of exit properties which have been truncated and re-adjusted to obscure geometric information about the turbine stage. The circumferential location of the sector of interest is defined by Φ and the size of each sector is defined by θ.

Torque, which is used to define actual work in the mechanical definition of efficiency, is measured using two redundant instrumentation systems: the torquemeter, highlighted in Figure 1 in purple, and the load cell on the water brake dynamometer, highlighted in Figure 1 in green. Photographs of these two systems are shown in Figure 4(a) and Figure 4(b) respectively. The calculated efficiency values as a function of the torque measurements from both of these systems will be presented for the remainder of this paper, highlighting the distinction from the thermodynamic definition of efficiency and the ability of the two calculation methods to detect the system performance using limited datasets.

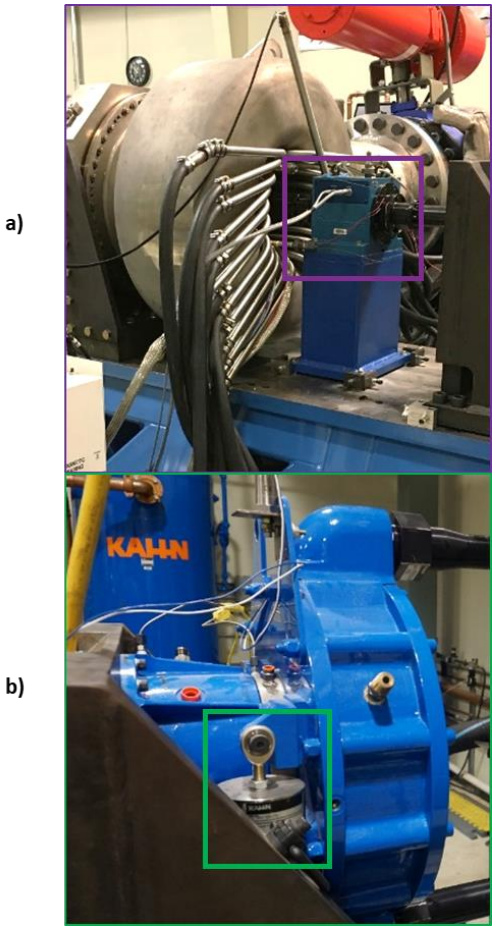

Figure 4. a) The torquemeter and b) the load cell attached to the water brake dynamometer which are used to measure torque.

Rig Builds and Operating Conditions

The data used in this paper come primarily from two different rig builds, each operating at the conditions specified in Table 2. These two rig builds, enumerated B_1 and B_2, ran using the same range of operating conditions but using a different set of blades. The ranges of the varied parameters across both of the rig builds featured in this study are given in Table 3, normalized by the baseline (BL) case. After these operating conditions have been set, the system is allowed to come to steady state over the course of several hours before data collection is initiated.

Measurement Uncertainty

The bias uncertainty is the fixed component of uncertainty, and can be described as a quantification of how far a measurement from a given instrumentation system is from the true value. It can also be propagated through a given calculation using these raw measurements with either the derivation method derived by Kline and McClintock [28] and used by Figiola and Beasley [35] or the perturbation method described by Moffat [26]. The bias uncertainty provides insight to which instrument is the source of the most error in the final calculation. Additionally, this study will use half of the calculated bias uncertainty as a threshold value for its reduction of precision uncertainty.

A calibration was performed for each measurement device contributing to efficiency calculations, including pressure transducers, thermocouples (TCs), resistance temperature detectors (RTDs), and the load cells on the torquemeter and dynamometer. In addition, relevant dimensions of each Venturi flow meter were confirmed with critical consideration of discharge coefficients. The bias of the MGP Venturi was calculated using the method developed by Stephens et al. [36].

Table 2. Turbine Operating Conditions

Parameter	Symbol	Value
Vane inlet Mach number	M_V	0.1
Vane inlet axial Reynolds Number	$Re_{V,x}$	1×10^5
Blade inlet axial Reynolds number	$Re_{B,x}$	1.4×10^5
Rotational Reynolds number	Re_Ω	$3.5\text{-}6.0\times10^6$

Table 3. Varied Parameter Ranges

Parameter	Range
$X_1/X_{1,BL}$	0.9-1.05
$X_2/X_{2,BL}$	0-1
$X_3/X_{3,BL}$	0-1
$X_4/X_{4,BL}$	0-1
$X_5/X_{5,BL}$	0.95-1

The biases of the thermodynamic property measurements were propagated through calculations of mass flow rate and enthalpy. For any value, such as mass flow rate, defined by an analytical expression, the partial derivative method derived from a Taylor series expansion was used. For properties such as enthalpy where an analytical representation was not available, thus requiring a lookup table or the application of the thermodynamic program REFPROP [37], the bias was propagated using a perturbation method, an application of a Monte Carlo simulation, the use of which was also demonstrated in Stephens et al. [36]. The discharge coefficient for the MGP and cooling stream Venturi flow meters were defined in accordance with ASME standards [38]. Ultimately, the bias uncertainties associated with the thermodynamic and mechanical definitions of efficiency were determined and are summarized in Table 4. The measurement uncertainties used to calculate these parameters are given in Table 5. Each value in this table is given as a percentage of the nominal measurement.

Precision uncertainty is the random component of uncertainty, and can be thought of as a measure of how far away the mean of a given dataset of a finite number of samples is from the hypothetical population mean or "true" system performance. Unlike bias, this value can be reduced through repeated measurements. This study uses a Student's t-distribution to quantify the precision uncertainty to a 95% CI using the relation given in Equation (1).

Table 4. Bias Uncertainty

Method	ε_b [points]
η_t	0.18
$\eta_{m,\,tqm}$	0.30
$\eta_{m,\,dyno}$	0.56

Table 5. Measurement Uncertainties

Parameter	Measurement Uncertainty
$\dot{m}_{MGP}$	0.27%
$\dot{m}_{TOBI}$	1.68%
$\dot{m}_{VTE}$	1.28%
$\dot{m}_{purge}$	2.12%
$T_{MGP,in}$	0.008%
$T_{MGP,out}$	0.008%
T_{TOBI}	0.03%
T_{VTE}	0.06%
T_{purge}	0.02%
$p_{MGP,in}$	0.03%
$p_{MGP,out}$	0.04%
p_{TOBI}	0.58%
p_{VTE}	0.43%
p_{purge}	0.92%
N	0.0029%
τ_{tqm}	0.23%
τ_{dyno}	0.61%

$$\varepsilon_p = t_{0.95}\frac{\sigma}{\sqrt{n}} \quad (1)$$

Here $t_{0.95}$ is the Student's t-distribution, which can be extracted from a table as a function of the desired CI and sample count, n. This is analogous to the z score for a Gaussian distribution.

EFFICIENCY DEFINITION

Thermodynamic and Mechanical Definitions

This study compares two versions of an enthalpy-based efficiency calculation: the thermodynamic method, η_t, where actual work is a function of enthalpy, and the mechanical method, η_m, where actual work is a function of torque and wheel speed. The expressions for these two formulations are given in Equation (2) and Equation (3), respectively.

$$\eta_t = \frac{\dot{m}_{MGP}\left(h_{t,MGP,1} - h_{t,2}\right) + \sum_j \dot{m}_{c,j}\left(h_{t,c,j} - h_{t,2}\right)}{\dot{m}_{MGP}\left(h_{t,MGP,1} - h_{t,2,s}\right) + \sum_j \dot{m}_{c,j}\left(h_{t,c,j} - h_{t,2,s,j}\right)} \quad (2)$$

$$\eta_m = \frac{2\pi N\tau}{\dot{m}_{MGP}\left(h_{t,MGP,1} - h_{t,2,s}\right) + \sum_j \dot{m}_{c,j}\left(h_{t,c,j} - h_{t,2,s,j}\right)} \quad (3)$$

In these equations, each j flow corresponds to one of the three implemented cooling flows in the START rig. The total enthalpies are calculated using REFPROP [37], with total pressure and total temperature as inputs. Ideal properties in the denominator are also calculated using REFPROP using an ideal expansion where change in entropy is set to zero. In Equation (3), N represents the wheel speed measured and τ represents the torque, measured using the two instrumentation systems shown in Figure 4. For the remainder of the paper, three calculations will be presented for each efficiency value: one using Equation (2) and two using Equation (3). Efficiency will also be presented in percentage points ranging from 0 to 100.

Sector-dependent Variations

To determine what the minimum sector size and optimal sector location is for the exit sector, efficiency was recalculated using every permutation of θ and Φ in accordance with Figure 3 for each of the three calculation methods and compared to the full 360° sector calculations for the thermodynamic method as a reference point. The efficiency values were also split into the two components: actual work and ideal work, which are plotted in Figure 5 and Figure 6 respectively. All of the following data originated from the B_2 rig build using the operating conditions from the baseline case.

The data shown in Figure 5 were calculated using the numerator from Equation (2) for Figure 5(a) and the numerator from Equation (3) for Figure 5(b) and Figure 5(c). The calculated work was normalized using the 360° value from the thermodynamic calculation as a reference point and then nondimensionalized using that maximum work rating. This maximum work rating was calculated using the maximum ratings for the torque (700 Nm or 516 ft lb) and speed (11,000 RPM) for the torquemeter used in this study. This normalization scheme, given in Equation (4), was used in order

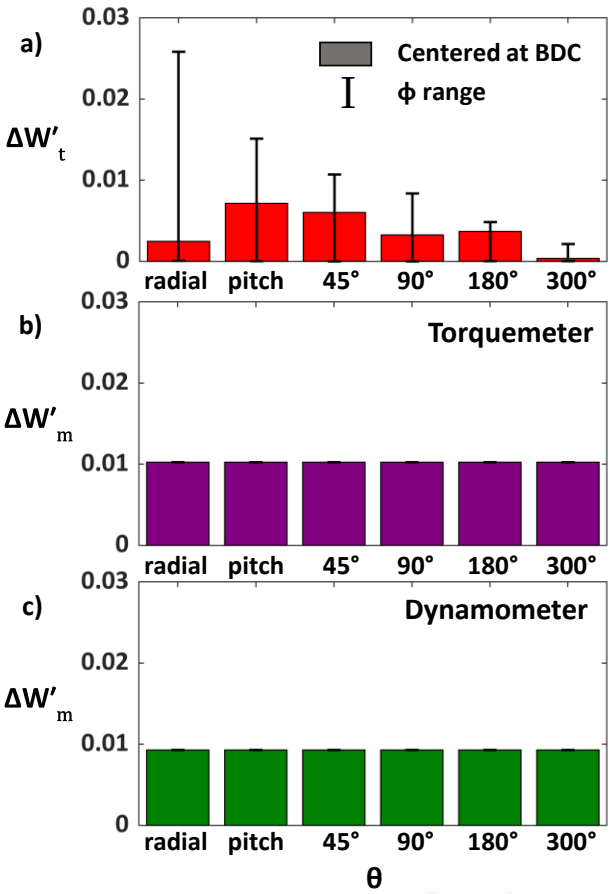

Figure 5. Actual work with respect to the full annulus thermodynamic definition as a function of several selected sector sizes with accompanying circumferential variation range bars for a) the thermodynamic method and the mechanical method using b) the torquemeter and c) the dynamometer.

to highlight the offset between the thermodynamic and mechanical definitions.

$$\Delta W' = \frac{|W - W_{t,360°}|}{2\pi N_{max}\tau_{max}} \quad (4)$$

The colored bars in Figure 5 represent the values calculated using only a limited section of the data available at the exit plane. The sector sizes examined here are one radial measurement, one vane pitch, 45°, 90°, 180°, and 300°. Each of these sectors was centered at bottom dead center (BDC) and the range of values from all other circumferential locations, Φ, is marked using black range bars.

In Figure 5, the first subplot shows variation in actual work using the thermodynamic method as a function of sector size and location, while the second two figures use the mechanical method measured using the torquemeter and dynamometer respectively. Figure 5(a) shows a significant amount of variation as well as a large offset from the mechanical methods while Figure 5(b) and Figure 5(c), the two mechanical methods, show no variation and only a small offset between each other.

One may note that in Figure 5(a), the Φ ranges decrease significantly as θ increases. This is because there is a significant amount of circumferential nonuniformity at the exit plane, as can be noted in Figure 3. Figure 5(a) shows the impact of only selecting small sectors – or even single radial measurements – when calculating actual work using the thermodynamic definition. For example, although the actual work from the radial measurement is not far from the full sector value, as evident from the relatively short bar in Figure 5(a), this value is very sensitive to its location and therefore to circumferential nonuniformities, as evident from the Φ range. This range is nearly five times as high as the bar itself, meaning the actual work calculated from a radial exit sector could have an offset from the full sector value that is five times as high depending on its circumferential location. Conversely, Figure 5(b) and Figure 5(c) show zero variation in actual work as a function of θ or Φ, because the mechanical definition does not use exit plane data for this value. Mechanical actual work is only a function of speed and torque, resulting in an integrated value that is independent of circumferential nonuniformity at the exit plane.

Figure 6 was constructed using an identical method to Figure 5, with the exception that the ideal work from the denominator of Equation (2) and Equation (3) is used. In Figure 6, all three plots are identical, including the value centered at BDC as well as the Φ ranges. This outcome occurs because the denominator of the thermodynamic and mechanical methods is identical and a function of enthalpy, which is therefore dependent on circumferential nonuniformity at the exit.

It is, however, not a coincidence that the range bars in Figure 6 appear to be narrower than the range bars in Figure 5(a). This is due to the way that the ideal enthalpy term at the exit plane, $h_{t,2,s}$ for the MGP and $h_{t,2,s,j}$ for the cooling paths from Equation (2) and Equation (3), is calculated. The isentropic, downstream enthalpy is calculated using REFPROP [37] only as a function of exit total pressure and inlet specific entropy. As a result, there are no terms in the ideal work expression which are a function of the exit plane temperature, only exit plane pressure. The sensitivity of the calculated efficiency to its pressure and temperature inputs was quantified in Figure 7.

Figure 7 was generated by recalculating efficiency and perturbing each input temperature and pressure by a given range that was representative of the variations that would be experienced during testing. The resulting relationships with each input temperature and pressure, $\frac{\partial \eta}{\partial T}$ and $\frac{\partial \eta}{\partial p}$, were determined and multiplied by the amount that each of those values realistically varies during a single test, ΔT and Δp, for Figure 7(a) and Figure 7(b), respectively. The labels on the x-axis refer to the flow stream or measurement plane, P, of each temperature (T) or pressure (p) measured efficiency input, where P_0 is upstream of the turbine inlet and P_2 is the turbine exit plane. The resulting values shown in Figure 7 demonstrate the sensitivity of efficiency to variation in each individual parameter within a single test.

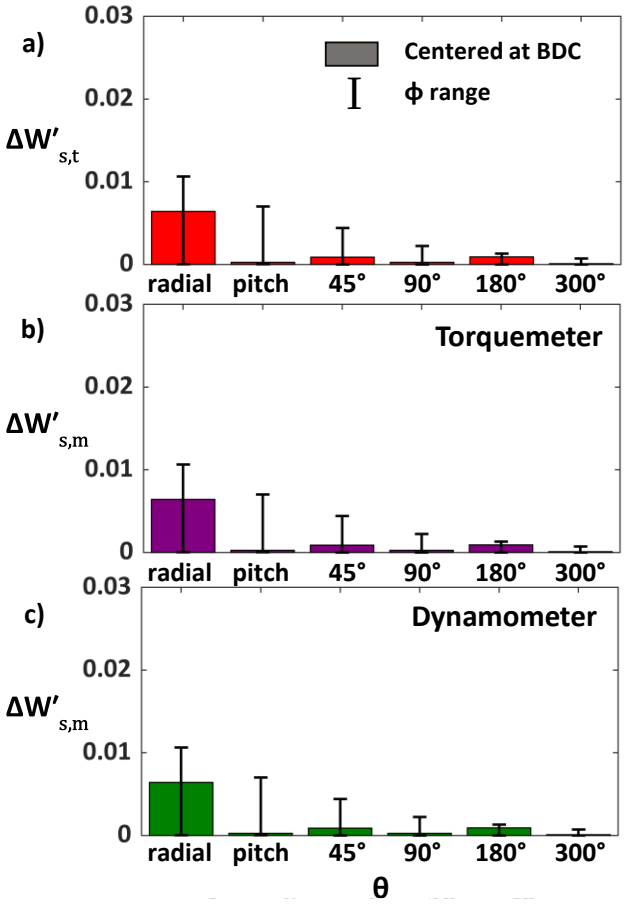

Figure 6. Ideal work with respect to the full annulus thermodynamic definition as a function of several selected sector sizes with accompanying circumferential variation range bars for a) the thermodynamic method and the mechanical method using b) the torquemeter and c) the dynamometer.

The leftmost bars in Figure 7(a) show that typical variations in the inlet temperatures have a nearly negligible impact on efficiency for the two mechanical methods, and a much smaller impact on the calculated efficiency than the exit variations for the thermodynamic method. Similarly, for the pressures seen in the leftmost bars in Figure 7(b), the pressure has identical impact between the three methods, but the impact from nonuniformities at the exit plane has more the twice the impact as the inlet plane nonuniformities. The other bars in Figure 7 also show that any variation in pressure and temperature from the other cooling streams have nearly negligible impact on the calculated efficiency.

The parameter with the greatest impact on efficiency is exit plane temperature, the circumferential variation of which can create a variation of nearly two efficiency points. As previously discussed, the mechanical method is not a function of exit plane temperature as the isentropic enthalpy used in the ideal work is only a function of exit pressure. For this reason, the noted dependence on temperature at the exit plane P2 in Figure 7(a) only exists for the thermodynamic method. In Figure 7(b), while the exit plane pressure influences all three

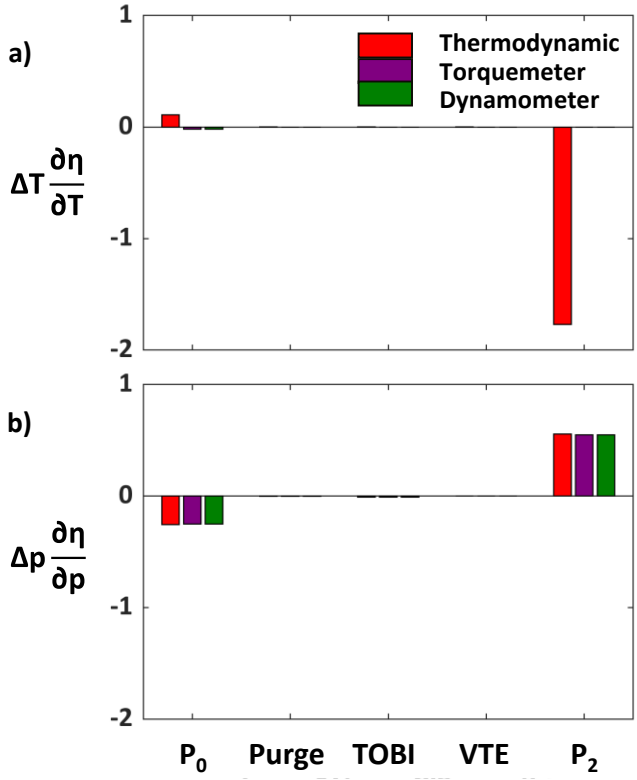

Figure 7. Variation in the final efficiency calculation as a function of a) temperature and b) pressure for each input to the equation.

methods in approximately equal proportion, this impact is less than one point and only half that of the exit temperature impact.

The range bars on Figure 5 and Figure 6 agree with the findings of Figure 7, showing that the parameter that is a function of exit temperature (actual work) will have a much higher dependency on sector size than the ideal work, which is a function of exit pressure only.

The result of combining the actual work and ideal work and examining efficiency as a function of sector size and location in summarized in Figure 8. The efficiency for all three plots in this figure is presented as the difference between each limited sector value and the full-annulus calculated value using the thermodynamic method according to Equation (5).

$$\Delta\eta = \eta - \eta_{t,360°} \tag{5}$$

While the decreasing range bars as a function of θ for both thermodynamic and mechanical efficiency methods show some dependence on circumferential location and therefore circumferential nonuniformity, the thermodynamic approach shows a stronger dependence than the mechanical methods. Additionally, the thermodynamic method in Figure 8(a) shows that the efficiency value itself also approaches that of the full-annulus 360° sector value as the sector size increases, as noted by the decreasing bar height. Unlike the range bars, this relation is not evident in the mechanical method, as the bar heights do not appear to significantly decrease in height with increasing θ in Figure 8(b) and Figure 8(c).

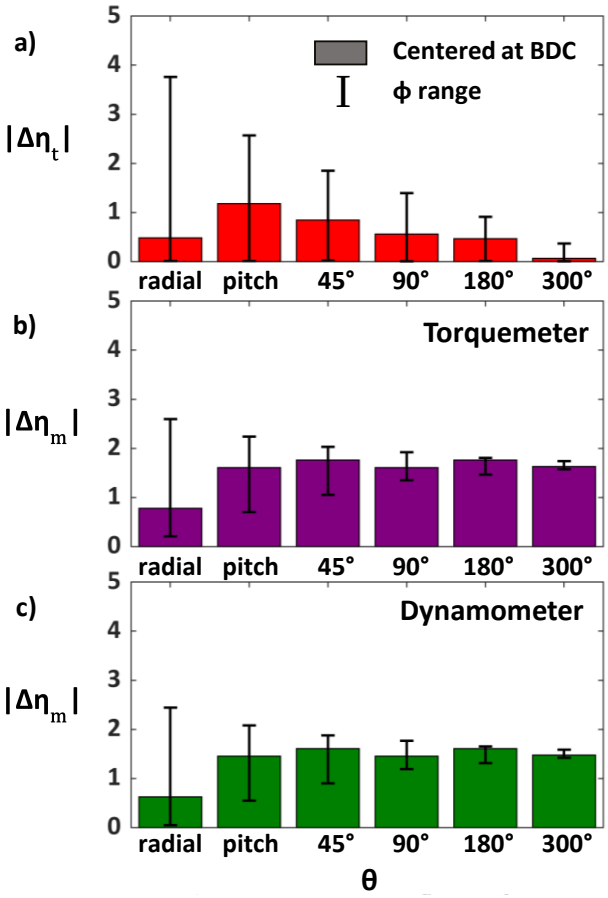

Figure 8. Efficiency with respect to the full annulus thermodynamic definition as a function of several selected sector sizes with accompanying circumferential variation range bars for a) the thermodynamic method and the mechanical method using b) the torquemeter and c) the dynamometer.

Notably in the latter two figures, while the two instrumentation systems agree with each other, they show a clear offset from the thermodynamic method in Figure 8(a) by up to two points. While the relatively small offset that was also noted in Figure 5 between the two mechanical methods can be simply attributed to bias between the two torque measurement instruments, there is a physical mechanism behind the offset between the thermodynamic and mechanical methods. A previous study by Neumayer et al. [16] also compared these two definitions and found approximately a 2% difference between the resulting efficiencies, which is on the same order of magnitude as the offset found in the present study.

The physical mechanism often attributed to this offset is disk friction and windage losses. Typically, a series of correction terms defined through empirical correlations [39,40] is applied to the mechanical definition of efficiency to prevent these secondary air system losses from being included in the performance assessment [15,30,34]. A distinct advantage of the thermodynamic method is that measurements are taken exclusively from the passage and therefore inherently only include entropy generation and losses from the turbine stage. Thereby the need for extensive correction terms is eliminated.

Based on the observed difference between thermodynamic and mechanical calculations, a study was conducted to determine if this offset is a matter of absolute value and potentially due to a calibration error, or if this was a fundamental problem in how work is being measured. Figure 9 shows the relation of the three efficiency calculation methods with a selection of independent parameters that were varied between the different operating conditions, as outlined in Table 2: X_1, X_2, and X_3. For each variable, the relation with efficiency was determined using a linear curve fit to get a relative slope, which are plotted as bars in Figure 9. The bars representing mechanical methods show similar relations between efficiency, across each of the three varied parameters. For the sensitivities outlined in Figure 9, an offset can be identified between the thermodynamic and mechanical methods. This means that there is not only an absolute value difference, but these two calculation methods are detecting losses at different rates depending on the varied parameter. Furthermore, the offset between thermodynamic and mechanical efficiency changes slightly for each of the parameters such that the thermodynamic method appears to generally be less sensitive for parameters X_1 and X_2, and slightly more sensitive for parameter X_3.

This inconsistency of sensitivities identified in Figure 9 may be due to a number of factors. For example, in the case of an injected cooling flow such as underplatform purge or blade cooling flow, the losses detected by the thermodynamic method would be due to the entropy generated by the mixing of and heat transfer between the coolant streams with the MGP. However, a mechanical method would detect additional losses due to windage from the impact of the flow on the rotor disk which would scale with the underplatform mass flow rate and swirl. In particular, when the flow is introduced into the wheel space using an axial hole, this mismatch in circumferential velocity between the disk and the flow would impose a shear force [41] and cause additional losses uncaptured by the thermodynamic method. Kuzke [18] cautioned on the subject

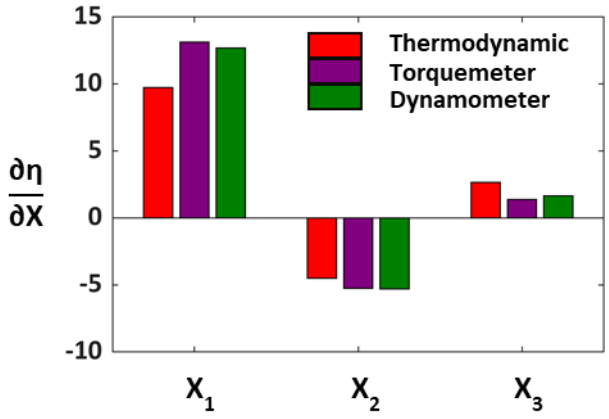

Figure 9. A comparison of slopes of efficiency as a function of a selection of varied operating conditions for each of the three calculation methods.

of the mechanical method of efficiency that power generated by the turbine is greater than that available at the shaft due to the windage and losses from accelerating the cooling air up to rotor speed.

Alternatively, a cooling flow such as VTE flow may create losses due to mixing and cooling, however it has also been shown to decrease the velocity deficit between the vane wakes and MGP flow, leading to a decrease in losses up to a certain flow rate [42,43]. Additionally, because this flow is introduced upstream of the rotor, the turbine can still use it to extract work [18]. Different aspects of this combination of effects may be captured to differing degrees by the mechanical and thermodynamic methods of monitoring performance.

The underlying source of the phenomena identified in Figure 8 and Figure 9 may be a combination of factors which require further analysis and investigation, to be provided by upcoming studies. Regardless, the presented value of efficiency can vary significantly, in both absolute value as well as relationship with operating conditions, depending on the definition selected. However, although the calculation method has these effects, the same trends in the linearized relationships with operating parameters in Figure 9 can still be observed and the same conclusions can still be drawn, regardless of method.

Both methods for calculating efficiency have advantages and disadvantages. The mechanical method includes extra losses from underplatform effects outside of the desired control volume requiring correlations to correct, but the thermodynamic method has been shown to have a strong dependence on the circumferential nonuniformities at the exit plane. To further quantify the degree of dependence on circumferential sector size, an optimal measurement method should be developed by finding the minimum exit plane sector size needed to best represent the system performance.

To find this desired optimal sector size, efficiency using the thermodynamic method as a function of θ centered at BDC was plotted for every individual baseline case test during rig build B_2 in Figure 10. The selection of thermodynamic method in the Figure 10 analysis is especially important because it correctly weights the circumferential variations at the exit plane due to their impact appearing in both the numerator and denominator. A similar analysis using the mechanical method, the circumferential nonuniformity trend will simply be the inverse of the denominator because the numerator is a constant.

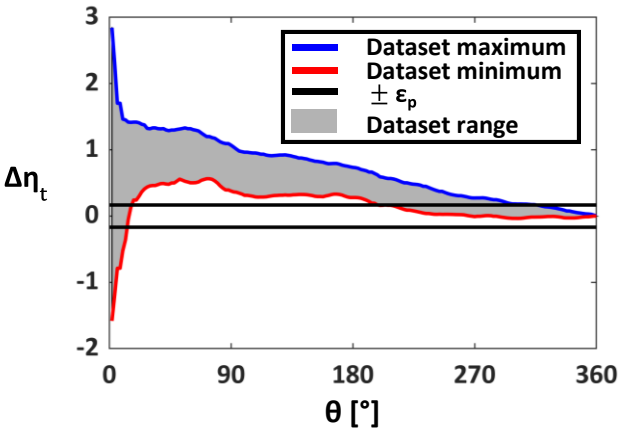

Figure 10. Efficiency as a function of sector size for all tests in a single test campaign as the values approach the full sector value.

In Figure 10, efficiency is presented using the method given in Equation (5). In total, 134 repeated tests are represented in Figure 10. The blue line represents the dataset maximum observed for all tests, and the red line represents the minimum. The gray section represents the dataset range between the minimum and maximum lines. To determine the minimum sector size necessary to be representative of system performance, precision uncertainty was calculated for each test. Rather than calculating the precision uncertainty using a sample of efficiency measurements for different tests, the sample was each radial measurement for a single test. Each test would then have an associated precision uncertainty, and the maximum precision uncertainty from the whole dataset was chosen to obtain the broadest range. In this way, the precision uncertainty range marked by horizontal black lines in Figure 10 represents a 95% confidence interval (CI) for the true performance of a single test.

As shown in Figure 10, the entire gray range enters the 95% CI of the 360° value when the sector is already about 300°. At this point, if the facility has the capability of creating a 300° sector, the full sector size may as well be used. It can also be noted that the gray range is neither randomly distributed nor centered about zero. Instead, a distinct peak around 0°, followed by a plateau up to a sector size of approximately 60° (centered about BDC), before steadily declining into the full sector value. The peak in variability at low sector sizes is contained within a region that is less than the width of a single pitch. This observation emphasizes expected behaviors that sector sizes less than an integer pitch values do not provide a meaningful or trustworthy estimate of performance.

The observed trend of asymmetric behavior in Figure 10 can also be directly correlated to the radially averaged exit temperature. Due to buoyancy and natural convection, the average temperature is higher close to top dead center (TDC) and is at its lowest at BDC. This general trend is also qualitatively visible in the polar contour in Figure 3, despite obscuring modifications. Figure 7(a) showed that the strongest influence on efficiency is a negative relation between exit temperature and efficiency. Therefore, the below-average temperatures around BDC result in local efficiency increases. The magnitude of this efficiency "boost" shown in Figure 10 aligns with the expectations established in Figure 7(a), albeit perhaps damped by the opposite trend in Figure 7(b).

One may note that the boosted plateau in efficiency is not precisely located at BDC, but just offset within 45°. This is attributed to colder temperatures accumulating at the bottom and being pushed in the direction of the motion of the rotor, in turn being displaced with a higher temperature flow. This change of temperature would align with the "boost" in efficiency of more than one point seen in Figure 10 based on the sensitivity of efficiency defined in Figure 7.

Ultimately, variation in the calculated efficiency value decrease incrementally as a function of sector size. Averaging larger amounts of the circumferential nonuniformities by using wider sectors will result in an efficiency value that is more likely to be the most physically representative estimate of performance. Whenever possible, one must use a 360° sector or risk misrepresenting the system performance. With this analysis, the greatest disadvantage to the thermodynamic method is resolved. Variability as a function of sector size is irrelevant when only full exit plane sectors are used as inputs to the efficiency calculation. Therefore, for future studies, the thermodynamic method of calculating efficiency will be implemented as the primary performance metric.

PRECISION UNCERTAINTY

All studies discussed so far in this paper lent credibility to individual measurements in terms of selected traverse sector size. However, one must also quantify the precision uncertainty associated with random error and data scatter. Equation 1 was applied to each group of data at different operating conditions for each rig build, such that one facility operating condition represented an independent dataset for analysis. It should also be noted that each dataset per specified operating condition was collected over the course of several days. To determine what minimum test count is required to adequately reduce the precision uncertainty, the precision uncertainty was calculated as a function of sample size. Using this method, each sample represents the efficiency of a single test's traverse measurement. For each sample size, n, spanning from two up to the total number of tests for each facility operating condition, 10 groups of n points were selected randomly from the available data. The precision uncertainty was then calculated for each group and plotted in Figure 11.

The threshold line represents half of the bias uncertainty for the thermodynamic efficiency method, as given in Table 3, or a value of 0.09 points. The individual markers represent the average precision uncertainty value from the 10 groups for a given sample size. The open circles represent sample sizes for which the calculated precision uncertainty for at least one of the 10 groups was above the defined threshold; filled circles represent sample sizes for which the calculated precision uncertainty of every group was at or below the threshold, which would denote that this sample size is large enough.

The minimum sample counts necessary from Figure 11 were collected for each dataset and are given in the histogram in Figure 12. The majority of test campaigns only require less than five tests, but there are several groups which require up to 10 repeat tests to yield a precision uncertainty less than the half-bias threshold. On average, four tests are necessary to meet the necessary performance metric. Based on these observations, standard procedures should be modified to take at least five good measurements at a given operating condition, but no more than 10 should be necessary. This figure allows testing strategies to be optimized by either ensuring that enough test time be dedicated to taking a sufficient number of measurements, or limiting the number of tests necessary to obtain an accurate measurement of efficiency.

The efficiency data presented as the difference with respect to the dataset mean for all available efficiency measurements per set of operating conditions from $B_{1,2}$ are shown in Figure 13. Overlaid on this plot are lines representing the bias uncertainty, in a solid line, and the minimum precision uncertainty from the available data, shown in the dotted line. The results from the studies presented in this paper provided the components, precision and bias uncertainties, to determine the total uncertainty for the presented efficiency calculations at the START facility. The bias is the fixed value given in Table 3 of 0.18 points. The precision uncertainty is dependent on the number of samples collected, but using the provided methods this has been shown to span from 0.09 points, representing half the bias uncertainty, down to a minimum of 0.01 points. Applying a root sum squared (RSS) expansion of these two

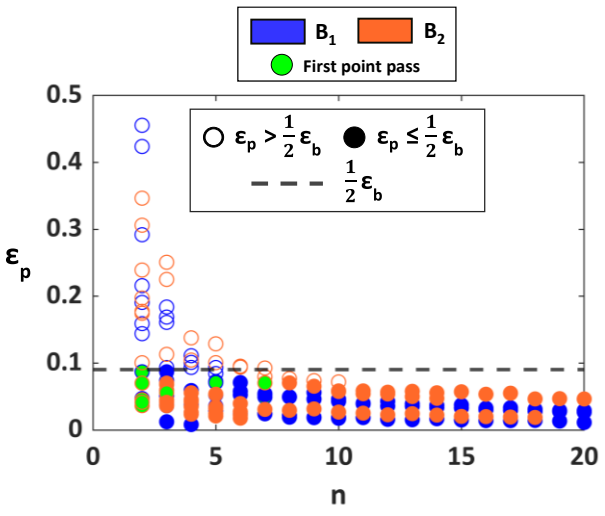

Figure 11. Precision uncertainty as a function of test count for all test campaigns as a function of sector size and depiction of pass/fail metrics.

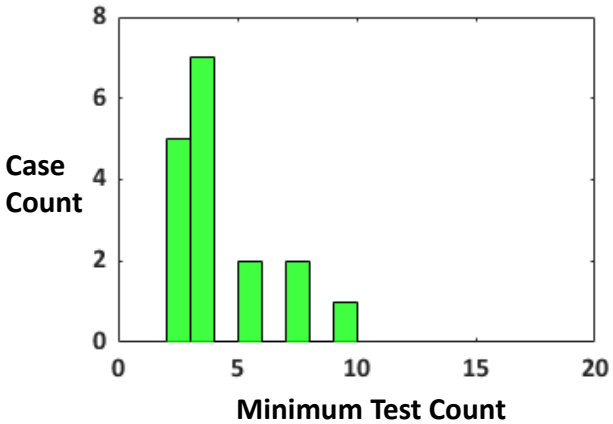

Figure 12. The minimum test count necessary to reach a precision uncertainty less than half of the bias uncertainty from all test campaigns.

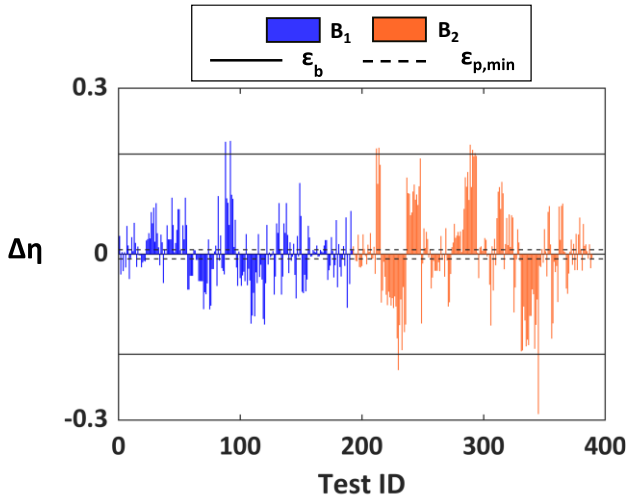

Figure 13. Calculated efficiencies from each test campaign relative to the respective average campaign performance.

contributors results in a total efficiency uncertainty ranging from 0.18 to 0.20 points.

CONCLUSIONS

This study examined several parameters with the intent of providing confidence in existing efficiency measurement procedures and streamlining future testing methods. Statistical analysis was used to determine the optimal equation to quantify stage efficiency, the optimal sector size for the exit plane input to the efficiency equation, and the number of individual measurements necessary for the presented efficiency to have a 95% confidence interval lower than half of the bias uncertainty. The findings from and methods developed in this study have a broad applicability not only for the START facility, but can be used to the development of other scaled turbine test beds as well as for the analysis of real engine performance.

To quantify stage efficiency of the single stage turbine at the Steady Thermal Aero Research Turbine Lab, two enthalpy-based equations for efficiency were examined: a thermodynamic method, where actual work is a function of enthalpy, and a mechanical method, where actual work is a function of torque and wheel speed. By comparing the variation in the calculated efficiency value as a function of sector size and location, as well as examining the slope of calculated efficiency as a function of a selection of operating points, it was determined that the thermodynamic method is more representative of the system. However, when smaller sector sizes are used for the thermodynamic integration at the turbine exit plane, the thermodynamic method can exhibit more variability than the mechanical method.

Precision uncertainty was applied to the calculated efficiency as a function of sector size where the exit sector input was centered at bottom dead center to determine the minimum sector size necessary to have a representative quantification of performance. It was determined that at least a 300° sector is needed to achieve a 95% confidence interval relative to the full 360° value. As a result, an ideal analysis should use as close to the full sector as possible. The use of a full sector also eliminates the primary disadvantage of the thermodynamic method of calculating efficiency.

The variations observed in efficiency as a function of sector size were related to circumferential nonuniformities in exit temperature and pressure. These variations can be partially attributed to buoyancy, leading to hotter sections at top dead center and cooler sections at bottom dead center. With this in mind, the impact of the temperatures and pressures at each inlet and outlet was quantified and related to the recorded change in efficiency over local maxima and minima in temperature.

A study was conducted to determine the minimum number of tests required for the precision uncertainty of the dataset to be less than half of the calculated bias uncertainty. On average, with the current methods and instrumentation, this facility would require at least five but no more than 10 tests to reliably meet this goal. This knowledge allows testing programs to be sufficiently characterized, while also operating efficiently to manage time spent at a single operating condition.

Finally, the total uncertainty for cooled turbine stage efficiency was calculated using a root sum square of the derived components of bias and precision uncertainty. Depending on the operating conditions and number of samples, this total uncertainty value spans from 0.18 to 0.20 points relative to the mean efficiency value.

To progress technology, turbine test rigs are necessary to elucidate small changes to turbine performance that, in fact, have impactful implications on climate changes by reducing the carbon footprint. It is therefore important that measurements of turbine efficiency are able to resolve incremental improvements through methodical back-to-back comparisons. This study walks through the steps to derive a precision uncertainty down to 0.01 efficiency points, which is indicative of the high quality of performance data generated at the START lab.

ACKNOWLEDGEMENTS

The authors are grateful to Pratt & Whitney for the support and collaborations needed to complete this research. This material is based upon work supported by the Department of Energy under Award Number DE-FE0025011. The authors would also like to recognize and thank Jeremiah Bunch for his critical contributions to rig maintenance, testing, and data acquisition.

thereof. The views and opinions of authors expressed herein do not necessarily state or reflect those of the United States Government or any agency thereof.

REFERENCES

[1] Bunker, R. S., 2017, "Evolution of Turbine Cooling," *GT2017-63205*.

[2] Reid, K., Denton, J., Pullan, G., Curtis, E., and Longley, J., 2006, "The Effect of Stator-Rotor Hub Sealing Flow on the Mainstream Aerodynamics of a Turbine," *GT2006-90838*.

[3] Schuepbach, P., Abhari, R. S., Rose, M. G., and Gier, J., 2010, "Sensitivity of Turbine Efficiency and Flow Structures to Varying Purge Flow," *J. Propuls. Power*, **26**(1).

[4] Denton, J. D., 1987, "Loss Mechanisms in Turbomachines," *93-GT-435*.

[5] Dahlqvist, J., and Fridh, J., 2016, "Experimental Investigation of Turbine Stage Flow Field and Performance at Varying Cavity Purge Rates and Operating Speed," *GT2016-57735*.

[6] Mohd Tobi, A. L., and Ismail, A. E., 2016, "Development in Geared Turbofan Aeroengine," *IOP Conference Series: Materials Science and Engineering*, **131**(1).

[7] Sato, A., Imamura, M., and Fujimura, T., 2014, "Development of PW1100G-JM Turbofan Engine," *IHI Engineering Review*, **47**(1).

[8] Young, J. B., and Wilcock, R. C., 2002, "Modeling the Air-Cooled Gas Turbine: Part 1-General Thermodynamics," *J. Turbomach.*, **124**(2), pp. 207–213.

[9] Yoon, S., Vandeputte, T., Mistry, H., Ong, J., and Stein, A., 2016, "Loss Audit of a Turbine Stage," *J. Turbomach.*, **138**(5).

[10] Zimmermann, R., Baar, R., and Biet, C., 2016, "Determination of the Isentropic Turbine Efficiency Due to Adiabatic Measurements and the Validation of the Conditions via a New Criterion," *Proc IMechE Part C: J Mechanical Engineering Science*, **232**(24), pp. 4485–4494.

[11] Hudson, S. T., and Coleman, H. W., 1997, "A Detailed Uncertainty Assessment of Measurements Used in Determining Turbine Efficiency," *AIAA 97-0776*.

[12] Louis, J. F., Hiraoka, K., and Masri, M. A. El, 1985, "A Comparative Study of the Influence of Different Means of Cooling on the Performance of a Combined (Gas and Steam Turbine) Cycle," *J. Eng. Gas Turb. Power*, **107**(1).

[13] Berdanier, R. A., 2022, "Calculating Cooled Turbine Efficiency with Weighted Cooling Flow Distributions," *GT2022-82365*.

[14] Horlock, J. H., and Torbidoni, L., 2008, "Calculations of Cooled Turbine Efficiency," *J. Eng. Gas Turb. Power*, **130**(1).

[15] Beard, P. F., Povey, T., and Chana, K. S., 2010, "Turbine Efficiency Measurement System for the QinetiQ Turbine Test Facility," *J. Turbomach.*, **132**(1).

[16] Neumayer, F., Jericha, H., Kulhanek, G., Seyr, A., Rossi, E., and Sanz, W., 2002, "Performance Testing of a First and a Second Transonic Turbine Stage," *GT-2002-30336*.

[17] Porreca, L., Behr, T., Schlienger, J., Kalfas, A. I., Abhari, R. S., Ehrhard, J., and Janke, E., 2005, "Fluid Dynamics and Performance of Partially and Fully Shrouded Axial Turbines," *J. Turbomach.*, **127**(4).

[18] Kurzke, J., 2002, "Performance Modeling Methodology : Efficiency Definitions ForCooled Single and Multistage Turbines," *GT-2002-30497*.

[19] Young, J. B., and Horlock, J. H., 2006, "Defining the Efficiency of a Cooled Turbine," *J. Turbomach.*, **128**(4).

[20] Seshadri, P., Duncan, A., Simpson, D., Thorne, G., and Parks, G., 2020, "Spatial Flow-Field Approximation Using Few Thermodynamic Measurements - Part II: Uncertainty Assessments," *J. Turbomach.*, **142**(2).

[21] Seshadri, P., Simpson, D., Thorne, G., Duncan, A., and Parks, G., 2020, "Spatial Flow-Field Approximation Using Few Thermodynamic Measurements - Part I: Formulation and Area Averaging," *J. Turbomach.*, **142**(2).

[22] Lou, F., 2022, "Approximating Gas Turbine Combustor Exit Temperature Distribution Factors Using Spatially Under-Sampled Meaurements," *GT2022-81623*.

[23] Barringer, M., Coward, A., Clark, K., Thole, K. A., Schmitz, J., Wagner, J., Alvin, M. A., Burke, P., and Dennis, R., 2014, "The Design of a Steady Aero Thermal Research Turbine (START) for Studying Secondary Flow Leakgaes and Airfoil Heat Transfer," *GT2014-25570*.

[24] Kline, S. J., 1985, "The Purposes of Uncertainty Analysis," *J. Fluids Eng.*, **107**(2).

[25] Castrup, H., and Ph, D., 2001, "Bias Uncertainty," *Integrated Sciences Group*.

[26] Moffat, R. J., 1988, "Describing the Uncertainties in Experimental Results," *Exp. Therm. Fluid Sci.*, **1**(1).

[27] Phillips, S. D., Eberhardt, K. R., and Parry, B., 1997, "Guidelines for Expressing the Uncertainty of Measurement Results Containing Uncorrected Bias," *J. Red. Natl. Inst*, **102**(5).

[28] Kline, S. J., and McClintock, F. A., 1953, "Describing Uncertainties in Single-Sample Experiments," *Mechanical Engineering*.

[29] Ferrero, A., 2020, "Uncertainty Propagation in Field Inversion for Turbulence Modelling in Turbomachinery," *IEEE*.

[30] Denos, R., Paniagua, G., Yasa, T., and Fortugno, E., 2006, "Determination of the Efficiency of a Cooled HP Turbine in a Compression Tube Facility," *GT2006-90460*.

[31] Haldeman, C. W., Dunn, M., Lotsof, J., MacArthur, C., and Cohrs, B., 1991, "Uncertainty Analysis of Turbine Aerodynamic Performance Measurementsin Short Duration Test Facilities," *AIAA-91-2131*.

[32] Keogh, R. C., Guenette, G. R., and Sommer, T. P., 2000, "Aerodynamic Performance Measurements of a Fully-Scaled Turbine in a Short Duration Facility," *2000-GT-486*.

[33] Schobeiri, M. T., Gilarranz, J. L., and Johansen, E. S., 2000, "Aerodynamic and Performance Studies of a Three-Stage High Pressure Research Turbine with 3-d- Blades, Design Point and off-Design Experimental Investigations," *Proceedings of the ASME Turbo Expo*, **1**(C), pp. 1–9.

[34] Atkins, N. R., Miller, R. J., and Ainsworth, R. W., 2004, "The Development of Aerodynamic Performance Measurements in a Transient Test Facility," *GT2004-53813*.

[35] Figiola, R. S., and Beasley, D. E., 2014, *Theory and Design for Mechanical Measurements*, *John Wiley & Sons, Inc., USA*.

[36] Stephens, J. E., and Kulkarni, S., 2020, "Calibration of a V-Cone for Low Mass Flows for Small Core Compressor Research," *GT2020-16140*.

[37] Lemmon, E. W., Huber, M. L., and McLinden, M. O., "NIST Standard Reference Database 23: Reference Fluid Thermodynamic and Transport Properites-REFPROP,

Version 10.0, National Institute of Standards and Technology, Standard Reference Data Program, Gaitherburg, MD."
[38] Miller, R. W., Lee, W. F. Z., and Wessely, K., 2004, *Measurement of Fluid Flow in Pipes Using Orifice, Nozzle, and Venturi.*
[39] Bulnes, F. K., Kerr, T., and Rimpel, A., 2022, "Calculating Windage Losses: A Review," *Proceedings of the ASME Turbo Expo*, **10**–**C**, pp. 1–13.
[40] Coren, D., Childs, P. R. N., and Long, C. A., 2009, "Windage Sources in Smooth-Walled Rotating Disc Systems," *Proceedings of the Institution of Mechanical Engineers, Part C: Journal of Mechanical Engineering Science*, **223**(4), pp. 873–888.
[41] Robak, C. W., Faghri, A., and Thole, K. A., 2019, "Analysis of Gas Turbine Rim Cavity Ingestion with Axial Purge Flow Injection," *GT2019-91807*.
[42] Aminossadati, S. M., and Mee, D. J., 2013, "An Experimental Study on Aerodynamic Performance of Turbine Nozzle Guide Vanes with Trailing-Edge Span-Wise Ejection," *J. Turbomach.*, **135**(3).
[43] Uzol, O., and Camci, C., 2001, "Aerodynamic Loss Characteristics of a Turbine Blade with Trailing Edge Coolant Ejection: Part 2- External Aerodynamics,Total Pressure Losses, and Predictions," *J. Turbomach.*, **123**(2).

